Porosities accessible to HTO and iodide on water-saturated compacted clay materials and relation with the forms of water: A low field proton NMR study

Gilles Montavon, Z. Guo, Christophe Tournassat, B. Grambow, D. Le Botlan

Porosities accessible to HTO and iodide on water-saturated compacted clay materials and relation with the forms of water: a low field proton NMR study

G. Montavon [1], Z. Guo [1], C. Tournassat [2], B. Grambow[1] and D. Le Botlan[3]***

[1] Subatech Laboratory, UMR 6457, Ecole des Mines / CNRS / IN2P3 / Université de Nantes, 4 Rue Alfred Kastler, 44340 Nantes, France

[2] BRGM, 3, Avenue Claude Guillemin, 45060 Orléans Cedex 2, France

[3] CEISAM, UMR-CNRS 6230, 2 Rue de la Houssinière, BP 92208, 44322 Nantes Cedex 03, France

* Corresponding author. E-mail address: *denis.lebotlan@chimbio.univ-nantes.fr*

** Present address: School of Nuclear Science and Technology, Lanzhou University, Lanzhou, 730000, China

Abstract

The aim of the present work was to quantify accessible porosities for iodide and for a water tracer (HTO) on water-saturated compacted clay samples (illite, montmorillonite and MX-80 bentonite) and to relate these macroscopic values to the forms of water in these porosities (surface/bulk water, external/internal water). Low field proton NMR was used to characterize and quantify the forms of water. This enabled the three different populations (structural OH, external surface and internal surface water) to be differentiated on hydrated clays by considering the difference in proton mobility. An accurate description of the water forms within the different populations did not appear possible when water molecules of these populations were in contact because of the occurrence of rapid exchange reactions. For this

reason, it was not possible to use the low resolution NMR method to quantify external surface and bulk water in fully water-saturated compacted clay media at room temperature. This latter information could however be estimated when analyzing the samples at –25°C. At this temperature, a distinction based on the difference in mobility could be made since surface water remained in a semi-liquid state whereas bulk water froze. In parallel, accessible porosities for anions and HTO were determined by an isotopic dilution method using capillaries to confine the materials. HTO was shown to probe the whole pore volume (i.e. the space made of surface and bulk water). When the surface water volume was mainly composed of interlayer water (case of montmorillonite and bentonite), iodide was shown to be located in the pore space made of bulk water. When the interlayer water was not present (case of illite), the results showed that iodide could access a small fraction of the surface water volume localized at the external surface of the clay particles.

1. Introduction

The Callovo-Oxfordian clay formation (COX) is currently being evaluated for the storage of high-level radioactive waste in France (Andra, 2005). The very low permeability and hydraulic conductivities of the clay barrier is expected to extend the lifetime of the waste packaging and slow down the consequent release of contaminants. Schematically, three different locations of water can be identified in water-saturated compacted clay systems (see Figure 1 or Appelo and Wersin, 2007). The first location corresponds to sufficiently large pores containing water molecules having physical and chemical properties similar or identical to bulk water free of any surface influence. The second water location corresponds to the vicinity of the external surfaces of mineral grains. These external surfaces can be sub-divided into basal surfaces or edge surfaces as a function of their localisation on a clay platelet. The third location corresponds to the interlayer of swelling clays. The water in the two latter

locations differs from the bulk water since it behaves similarly to water in a concentrated ionic solution arising from the electrostatic double layer generated by the surface charge of the material (Sposito and Prost, 1982). Indeed, the cation concentration in the interlayer is about 4 M. Finally, structural water or structural OH groups in the clay crystals, which does not take part in any exchange with the environment, also needs to be mentioned.

The transport of trace elements (e.g. radionuclides) in consolidated, water-saturated porous clay systems is controlled by sorption and repulsion and by diffusion processes (e.g. Andra, 2005; Bradbury and Baeyens, 2003a; Yu and Neretnieks, 1997) and knowledge of the porosities accessible to the different contaminants is a prerequisite for the development of transport models. The contaminants behave differently according to their localisation (Appelo and Wersin, 2007; Appelo et al., 2008). In the bulk water, both cations and anions can be transported by diffusion and are not affected by the surface. The water located at a typically negatively charged surface is accessible to cations as sorbed species whereas the anions, like halogenides, cannot access either the interlayers or the largest part of the electric double layer developed at the external surface of the clay, for electrostatic reasons. This behaviour is qualified as the "anionic exclusion" effect (e.g. Sposito, 1992). Bradbury and Baeyens (2003b) have also shown that knowledge of the volume fraction of the pore space accessible to chloride is important for understanding the pore water chemistry of bentonite. Finally, knowledge of the volume fraction of the pore space located in interlayer nanopores is important for understanding the diffusion of water tracers in bentonite (Bourg et al., 2006).

The water content in the interlayer space can be experimentally characterized by X-ray diffraction looking at the spaces between the basal faces (e.g. Sato et al., 1992) or modelled by molecular dynamic approaches (Tambach et al., 2004; Chavez-Paez et al., 2001). The number of water layers in the interlayer depends on the nature of the interlayer cations and on the compaction degree (Kozaki et al., 1998; Ferrage et al., 2005). The external surface water

structure and properties can be probed by a molecular dynamics study showing significant density oscillations up to three water layers at phyllosilicate mineral surfaces (Greathouse and Cygan, 2006; Wang et al., 2006; Marry et al., 2008; Tournassat et al., 2009b).

Low field NMR (LF-NMR) is another technique that enables the forms of water to be quantified and characterized. Its low field limits the field gradient inside heterogeneous samples, in particular in porous media (Guichet et al., 2008, Mitchell et al., 2008), while the short 90° RF pulse width used enables protons of both solid and liquid phases to be excited. Short, interesting introductions to NMR and LF-NMR have been presented by Manalo et al. (2003), Todoruk (2003) and Mitchell et al. (2008). For a given type of sample, relaxation times are a function of the mobility of the protons and therefore enable a quantitative characterization of water, especially between ice and non-freezing water. Such a technique therefore appears interesting to use in the context of the study, i.e. to characterize the different forms of water (Figure 1). For instance, Nakashima (2004) studied the NMR properties of water on gels of Kunigel-VI bentonite, but the high bulk water content in the sample (water content above 62.3 %) did not allow an accurate description of the surface water. LF-NMR is also used in food science (e.g. Bertram et al., 2001, Hills, 2006), in the petroleum sector (e.g. Al-Mahrooqi et al., 2006, Guichet et al., 2008), for cryoporometry (Mitchell et al., 2008) or to study the diffusion of water in cement paste (Hansen et al., 2005).

LF-NMR was tested in the present study to assess whether it can be used to characterize the forms of water in water-saturated compacted clay media. Both model mineral phases of interest (synthetic montmorillonite, illite) and MX-80 bentonite were used. The results were compared with accessible porosities estimated for iodide and HTO using an isotopic dilution method (Montavon et al., 2006).

2. Materials and methods

2.1. Materials

All chemicals were of analytical purity. Radiotracers were obtained from CERCA (French Nuclear Fuel Research Centre). Two model phases were used: a synthetic montmorillonite (SM) (Reinholdt et al., 2005) and illite from Le Puy in France (ILL) (Gabis, 1958). The latter was purified to remove calcite (11% by weight) by adjusting the pH of a clay suspension to 3 with HCl. Calcite dissolution was considered finished once the pH did not vary for one night (variation less than ±0.05 H unit). Model phases were prepared in the Ca- (Ca-SM), Na- (Na-SM) and "Na"- (Na-ILL) forms. In addition to the two model phases, MX-80 bentonite (MX-80) was studied. Before use, MX-80 was equilibrated with a solution having a cation composition close to that of the claystone of the Callovo-Oxfordian site ($[K^+]=4.10^{-4}$ M, $[Ca^{2+}]=6.10^{-3}$ M, $[Mg^{2+}]=3.10^{-3}$ M, $[Na^+]=4.10^{-2}$.M, $[Cl^-]=5.8.10^{-2}$ M) (Gaucher et al. 2006). The cation exchanger composition estimated in equivalent fraction with the model of Tournassat et al. (2009a) amounted to 18, 56 and 23% for Na, Ca and Mg, respectively. A low content of K was not considered in the calculation. The characteristics of the clay materials are given in Table 1. The specific surface area of the SM powder sample was measured by the Brunauer-Emmett-Teller (BET) method, using a 7-point N_2 adsorption isotherm. The edge surface area was determined by AFM (atomic force microscopy) measurements (Marty et al., 2009). For illite, both edge and basal surfaces were determined from high resolution gas adsorption isotherms measured in conditions given in Bardot et al. (1998).

Montmorillonite total surface area is given by the sum of the external basal surface, interlayer surface and edge surface. External and interlayer surfaces (SS_a in what follows) is directly linked to M_{clay}, the mass of a crystallographic clay cell (of surface area S_{ab}). Bourg (2004) compiled S_{ab} values for natural montmorillonites and found a mean value of 46.4 ± 0.4 $Å^2$. Formula weights of montmorillonites depend principally on their iron content and the charge

compensating interlayer cations. There are little variations of their formula weight and Bourg concluded to a value of 746 ± 1 g mol^{-1}. With these values, SS_a can be calculated according to:

$$SS_a = 2 \times \frac{S_{ab} \times N_A}{M_{clay}} = 749 \ m^2 \ g^{-1} \quad (1)$$

This value is used to estimate the interlayer surface for both synthetic and natural montmorillonites (see Table 1).

2.2. Sample preparation

2.2.1. Dry samples

Dry samples were prepared for NMR measurements to probe structural OH groups. Only the model phases were used (Table 2). They were obtained by drying the materials at 125°C for 24 hours and 105°C for 48 hours for illite and synthetic montmorillonite, respectively. These samples were measured either in a dry atmosphere (water activity (aw) ~ 0) or in the presence of D_2O. In the latter case, D_2O was added to the sample (about 50 % by weight) and the exchange process was monitored over time. One day was enough to reach an equilibrium state.

2.2.2. Hydrated samples

Hydrated samples were prepared for NMR studies, either to calibrate the data for the quantitative analysis (Figure 2) or to characterize the forms of water. In the latter case, conditions were chosen to assure the samples were nearly fully hydrated (see part 2.3.3.) to try to distinguish between the different types of surface water molecules (Table 3). Samples were prepared by hydrating dry material in humid atmosphere (aw = 1) until the target water content (by weighing) was reached. Once obtained, the material was transferred to the NMR tube and the relaxation curves were measured periodically to assess the repeatability of the

measurements. The water content in the samples is given in percentage with respect to the wet material according to the relation:

$$Wc = \frac{m_{H20}}{m_{tot}} \quad (2)$$

where m_{tot} and m_{H20} are the mass of the hydrated sample and the mass of surface water, respectively.

2.2.3. Consolidated, water-saturated porous media

For these samples, both surface and bulk water exist. They were prepared for both microscopic (NMR experiments) and macroscopic (isotopic dilution experiments) measurements. The compacted medium was prepared in capillaries according to the method given in Montavon et al. (2006) (see next part). The percentage water was determined according to eq. 2 knowing the mass of the water-saturated material and the mass of water determined by NMR (Free Induction Decay signal) and/or using tracer experiments with HTO. A list of the samples is given in Table 4.

2.3. Experimental procedures

2.3.1. Porosity measurements in the consolidated states

Teflon capillaries (1.4 mm internal diameter) were used as supports to compact the material. The mass of compacted material amounted to 3 ± 1 mg and 20 ± 2 mg for isotopic dilution and NMR experiments, respectively. These capillaries containing the compacted material were then brought into contact with an external solution to saturate the pores (external volume, V_{ex}, of $0.5.10^{-6}$ m^3 per capillary). For NMR experiments, the capillaries were then directly placed in the NMR tube. For the isotopic dilution method, after addition of I-131 or HTO to the external solution, the system was allowed to equilibrate until the total measured radioactivity in the water-saturated compacted material was constant over time. This represents the sum of the radioactivity in the pore water and the radioactivity adsorbed on the

material. For some experiments, natural iodide was added to the external solution. If the adsorption can be neglected and assuming that the radioactivity concentrations (in Bq/m^3) in the external solution and pore water are identical, the volume probed by the radionuclide (V_p) could be calculated according to the following equation:

$$V_p = \frac{A_{tot}}{A_{ex}} V_{ex} \quad (3)$$

Where A_{tot} and A_{ex} are the radioactivities (in Bq) measured in the water-saturated compacted material and external solution, respectively. At least 6 experiments were performed in parallel and the values given in the paper are the mean values with the associated standard deviations. Analysis of the diffusion process, i.e. the evolution of A_{tot} over time, was performed using the PHREEQC calculation code (Parkhurst and Appelo, 1999).

2.3.2 NMR measurements

Low field (LF) ^{1}H NMR methodology: The inhomogeneity of the permanent magnetic field of LF-NMR devices gives rise to very large peaks so that chemical shifts are no longer exploitable. The occurrence of paramagnetic impurities in raw natural clays also produces large peaks in high resolution (HR) NMR, and decreases the relaxation time of protons in their vicinity; this explains why HR-NMR studies are carried out on synthetic clays. The observable parameters with LF-NMR devices are apparent relaxation times, T_2^*, determined from Free Induction Decay (FID) signal obtained after a single 90° RF excitation pulse. Quantitative information can be obtained when all the protons are excited with the same power. According to the set-up of the apparatus (length of the PW90 pulse), such information can be obtained provided that the protons have T2* values above 30 µs. True relaxation times, T_2 were determined from spin-echo relaxation curves and measured using the CPMG (Carr-Purcell-Meiboom-Gill) sequence (Meiboom and Gill, 1958): 90°x-(τ-180°y -2τ-180°y -τ-

Acq.) n'. They are related to the mobility of protons, i.e. the more mobile the proton, the higher the relaxation.

NMR acquisition parameters: NMR measurements were performed using a Maran Ultra (Oxford Instruments) NMR device, 23.2 MHz, using a 10 mm thermostated probe, with 90° and 180° pulse widths of 3.5 and 7.0 μs, respectively. FID signals were sampled with the following acquisition parameters: dwell time, 0.1 μs, taking up to 31000 data points and averaged over 100 to 1000 acquisitions with a relaxation delay of 2 s. The pulse spacing time τ used in CPMG spin-echo sequences was 30 μs; this short pulse spacing time limits the effects of the internal field gradient on T_2 measurements (Snaar and Hills, 1995). The number of measured echoes, n', between 500 and 5000, was chosen in order to sample the complete decay of the relaxation signal. For the quantitative analysis of the data, a calibration was performed with MX-80 and ILL (Figure 2) to relate the intensity of the total NMR FID signal, I (in arbitrary units, a.u.), to the water content, Wc (eq. (2)). The following relation was obtained in the 0-40% range of water content: $I = b*Wc+I_0$, with b=84.5 (r^2=0.998) and I_0 corresponding to the signal of the dried sample.

The repeatability of the FID signal and CPMG relaxation curve measurements was systematically studied using three / four NMR tubes prepared from the same sample of hydrated clay. The deviation of the signal intensity, which is related to the number of protons probed, was below 2%.

NMR relaxation curve treatment: As shown previously, the FID signal in an inhomogeneous magnetic field is Gaussian in shape (Le Botlan and Ouguerram, 1997) according to:

$$I(t) = \sum_i I_i \cdot \exp\left[-\left(\frac{t}{T_{2i}^*}\right)^2\right] \quad (4)$$

where T_{2i}^* is the apparent T_2 of the ith component whose intensity is I_i; a T_2^* of 5-30 μs indicates a solid phase, 50-200 μs a semi-liquid phase and T_2^*>1000 μs a "very free" water.

For $T_2^* \geq 200$ μs, true T_2 are obtained using a spin-echo sequence. The relationship between apparent T_2^* and true T_2 relaxation times is given by (Abragam, 1961):

$$\frac{1}{T_2^*} = \frac{1}{T_2} + \frac{1}{T_{2inh}} \quad (5)$$

When $T_2 >> T_{2inh}$, then $T_2^* \approx T_{2inh}$; the T_2^* values greater than about 1000 μs correspond to the inhomogeneity parameters of the magnetic field ($T_{inh} \approx$ 1.5-3 ms), and their total intensity corresponds to the very liquid phase.

The CONTIN Program (Provencher, 1982, Kowalczyk et al., 2002) was used to deconvolve FID (T_2^*) or CPMG (T_2) relaxation curves, to obtain "continuous" distributions of relaxation times according to:

$$I_t = \sum_{i=1}^{350} I_i \exp(-t/T_{2i}) \quad (6)$$

The program determines the intensity I_i of 350 imposed T_{2i} values within a given range and increasing in a geometrical manner. The NLREG program (Dennis et al. 1981) was also used to determine discrete T_2 components:

$$I_t = \sum_{i=1}^{n} I_i . \exp(-t/T_{2i}) \quad (7)$$

the number n of components, between 1 and 3, was adjusted to obtain a scattered distribution of residuals. An example of residuals obtained for the fitting of the CPMG curve of MX-80 powder (14% water content) is given in the supplementary information.

The limitation of these methods depends on the ability of mathematical treatments to differentiate two components whose relaxation times are in a ratio lower than 1.5-2 (Mitchell et al., 2005) and according to the signal/noise ratio. In our case, the signal/noise ratio was about 1000 and T_2 and intensity parameters were obtained in a range of ± 5%.

The system was first tested with a bentonite sample (water content of 66% by weight). A T_2 of 10.5 ms was determined (pulse spacing time $\tau=200$ µs to be in the same acquisition conditions as Nakashima, 2004). The value is in very good agreement with that of 10.2 ms obtained with Kunigel-V1 bentonite (water content of 62.3%) at 20 MHz (Nakashima, 2004). For comparison, at 25°C, the T_2 relaxation time for the synthetic ground water is T_2=2.44 s.

2.3.3. Characteristics of the water-saturated compacted clay media

We report in this part the different calculations made in the paper, and especially in Table 4, and how the uncertainties were calculated. In all cases, we consider the volumetric mass of water (ρ_{H_2O}) in the compacted state equal to 1000 kg/m^3. The dry mass of clay was calculated considering the water content determined by NMR.

The dry density corresponds to the dry mass of the clay material divided by the volume occupied by the water-saturated compacted medium. It was calculated according to:

$$d=\frac{m_{tot}(1-Wc(NMR))}{h.\pi r^2} \quad (8)$$

Wc(NMR), m_{tot}, h and r correspond to the water content determined by NMR, the weight and the height of the water-saturated compacted clay medium and the radius of the capillary, respectively. The error associated with d was calculated according to the relation:

$$\frac{\sigma_d}{d}=\sqrt{\left(\frac{\sigma_{Wc}}{1-Wc}\right)^2+\left(\frac{\sigma_h}{h}\right)^2+\left(\frac{\sigma_{m_{tot}}}{m_{tot}}\right)^2} \quad (9)$$

The compaction homogeneity for the long capillaries prepared for the NMR studies was checked by analyzing dry density profiles with sample slices of about 2 mm in height. The density was shown not to be affected by the contact times between the compacted medium and the external solution (1-60 days) showing no significant swelling once the system was saturated with water. The corresponding total porosity in the porous media, calculated using

the densities of the materials, varied between 0.53 and 0.78 (Table 4). For SM, the porosity was relatively important and the sample should be considered as a gel rather than in a compacted state.

The total porosity refers to the volume occupied by the surface and the bulk water divided by the total volume occupied by the water-saturated porous clay system. It can be theoretically calculated considering the volumetric mass of the clay (ρ_{clay}) and the dry density of the compacted system:

$$P = \frac{\rho clay - d}{\rho clay} \tag{10}$$

With associated error $\frac{\sigma_P}{P} = \frac{\sigma d}{d}$ (11)

It can also be calculated using the water content experimentally determined with HTO (isotopic dilution method) or by NMR (FID signal) considering ρ_{H_2O}=1000 kg/m^3. In this case:

$$P = \frac{\frac{Wc}{\rho H2O}}{\frac{Wc}{\rho H2O} + \frac{(1-Wc)}{\rho clay}} \tag{12}$$

with $\frac{\sigma_P}{P} = \sqrt{(\frac{\sigma_{Wc}}{1-Wc})^2 + 2(\frac{\sigma_{Wc}}{Wc})^2}$ (13)

The surface water is given as the water content (mass of water divided by the mass of the sample, Wc) or as the mass of water (in g, defined as gw in the text) per kg of dry clay (defined as kgclay in the text). The data were given as well in terms of water layers at the surface considering:

i. Three hydration layers bound to the external surface (working hypothesis; for instance, Sposito and Prost, (1981) reported that the water content at which the last

added increment of water has the same infra-red spectroscopic characteristics, i.e. band position, intensity and profile, as bulk liquid water corresponds to 2-3 layers of water in Na-hectorite).

ii. Three and two layers associated with the interlayer ions Na^{+},Ca^{2+} and Mg^{2+}, respectively for SM and MX-80 (Kozaki et al., 1998; Van Loon et al., 2007; Cases et al., 1997, Ferrage et al., 2007; Melkior et al., 2009). Since Na/Ca-smectites tend to segregate into a mixture of Na-smectite and Ca-smectite (Iwasaki and Takashi, 1988), the mean coverage in the interlayers was calculated according to the following relation:

$$\bar{n} = X_{Na} n_{Na} + X_{Ca} n_{Ca} + X_{Mg} n_{Mg} \quad (14)$$

where X_i represents the cation exchanger composition estimated in equivalent fraction;

iii. A water layer thickness value of 0.3 nm. For MX-80 bentonite, secondary phases were not taken into account: the contribution of secondary phases to the external and total surfaces represents only 6 and 0.3%, respectively (Andra, 2005).

2.4. Analytical Methods

I-131, Cl-36 and H-3 were analyzed by liquid scintillation counting using a Packard 2550 TR/AB Liquid Scintillation analyzer. The scintillation cocktail was ULTIMA GOLD AB™ (PACKARD). The SM surface was measured using the apparatus ASAP 2010 from MICROMERITICS. Height and mass of water-saturated or dry compacted clay media were determined using an electronic MAHR 16EX caliper (0.01 mm accuracy) and a SORTORIUS ME215P balance (0.01 mg accuracy).

3. Results and Discussion

3.1. NMR results

3.1.1. NMR results on dry samples

The analysis of the FID signal of a Na-illite or a Na-smectite sample gave two populations: one with a very short T_2^* value of about 20 μs (population I), the other characterized by a distribution of longer T_2^* varying between 50 and 150 μs (population II) (Table 2).

When D_2O is added to the sample, it becomes possible to distinguish between exchangeable and non-exchangeable protons in a given population, owing to changes in mobility in the sample. Thus, the exchanged protons in D_2O achieve a higher mobility (long relaxation time) due to an increase in the amount of liquid phase while the non-exchangeable protons remain associated with the solid phase with an almost identical relaxation time. Typical relaxation curves are presented in Figure 3 for the synthetic Na-saturated montmorillonite.

The results given in Table 2 show that the protons of population I are mainly non-exchangeable. The mobility of its protons is very weak. They should therefore correspond to protons of structural OH groups. Based on FTIR (Fourier Transform Infrared) measurements, Tournassat et al. (2004) have shown that these structural OH groups are not likely to exchange with D_2O at 25°C in a timescale comparable to the one used in the present study i.e. several days at room temperature. The quantitative analysis of the data leads to an estimation of about 3.5 moles of non-exchangeable H per kg of dry clay (Table 2). The structural formula (Table 1) enables a ratio of 4.97 moles of structural OH per kg_{clay} to be calculated. The underestimation of the experimental value is due to the very short relaxation times (16-21 μs) compared to the length of the 90° RF pulse, 3.5 μs (Ernst et al., 1987); this leads to an experimental correction coefficient of about 1.4 for the intensities of this T_2 range.

As can be seen, a small fraction of population I is exchangeable. These protons may be associated with surface OH groups at the edges of clay platelets. According to the literature

(Bradbury and Baeyens, 1997; Bradbury and Baeyens, 2005), illite edges exhibit surface groups similar to those of montmorillonite. Taking into account an edge surface area of 26 m^2/g for the Na-illite (Table 1), the 0.4 x 1.5 mole of H/kg_{clay} (Table 2) of exchangeable protons of population I corresponds to 13.9 H/nm^2. This value is commensurable with the reactive site density value proposed by Bourg et al. (2007) or Tournassat et al. (2004) for clay edge surfaces (10.3 and 13 site/nm^2 respectively). One can conclude that the exchange rate between edge site OH groups and adjacent water molecules is fast. The protons associated with population II ($50\ \mu s < T_2^* < 150\ \mu s$) were completely exchangeable by deuterium and would thus correspond, in the dry sample, to protons of some residual water molecules, bound to the surface. The amount of this residual bound water corresponds to 0.75 H per kg_{clay} i.e. 6.75 g water per kg of illite. Considering the external basal surface area of illite particles (104 m^2/g), this 6.75 gw /kg_{clay} corresponds, on average, to about 2.2 H_2O/nm^2.

For synthetic Na-montmorillonite, considering an edge surface area of 11 m^2/g (Table 1), the 0.6 mole of H/kg_{clay} (Table 2) of exchangeable protons, corrected by a coefficient of 1.4 as explained above for illite, corresponds to 46 H/nm^2. This value is above the value expected from crystallographic considerations (Tournassat et al., 2004; Bourg et al., 2007) pointing to the presence of either additional sites not located on the edge (e.g. due to defects in the structure of this poorly crystallized synthetic material) or to remaining hydration water molecules in the interlayers not exchanged in the time scale of the experiment. The presence of water molecules left in the interlayers is further in agreement with the higher amount of exchangeable water (populations I and II) quantified as compared to illite. This is in agreement with the work of Alba et al. (2003) who reported a minimum temperature of 150°C to achieve the complete disappearance of the proton signal from interlayer water (a temperature of 105 °C was fixed in the present study). Knowing the adsorption isotherm of water on Na-montmorillonite (Michot et al. 2002), the water content determined in the study

corresponds to a relative humidity RH of less than 5%, thus confirming the dryness of the atmosphere used in our experiments.

Finally, surface water molecules can be bound to different metal ions with different coordination arrangements (Zhuravlev, 2000). These different environments affect T_2^* values (Nakashima, 2004). Therefore, the presence of a distribution of T_2^* values associated with population II is not surprising although a more accurate interpretation of the experimental data remains problematic.

In the following, the signal arising from structural OH-groups (experimentally determined) is systematically subtracted from the total FID signal for the determination of the water content.

3.1.2. NMR results on hydrated samples

The exponential analysis of CPMG relaxation curves for the 8.8% Wc illite sample gave a single T_2 relaxation time value (Table 3); these 8.8% water contents (96 g_w/kg_{clay}) correspond roughly to 2.5 layers of water on average on the whole external surface area of the particles (130 m^2/g). Given the single measurable T_2 component, the water molecules in the first monolayer, which have their own surface relaxation time, are in rapid exchange with the water molecules of the other layer(s) (Zimmerman and Brittin, 1957, Barrie, 2000, Mitchell et al., 2005). The characterization of the individual layers is therefore not possible by T_2 relaxation time measurements, at room temperature, when these populations are in contact. The observed relaxation rate corresponds to the weighted average of the relaxation rates of the water molecules in the different layers. The exchange rate is therefore faster than the NMR time scale (25-30 μs) as observed with Vycor glass (Hirama et al., 1996) and porous silica gels (Korb et al. 2003, Porion et al. 1998), but contrary to that observed with some biological materials such as starch (Le Botlan et al., 1998) or membranes by a femtosecond time-resolved study (Ghosh, 2007). This phenomenon was not foreseeable from the studies on

water-rich gels of Kunigel-V1 bentonite (Nakashima, 2004) because bulk-like water was in a very great proportion in the studied samples. In addition, this result is in agreement with the absence of interlayer water in illite, leading to a single T_2 component for the water located on the external surface of the particles.

For MX-80 bentonite, three T_2 values were obtained. An experiment performed as a function of temperature (from 2°C to 60°C) showed an increase in the relaxation times but with the same ratios and without modification of the widths (data not shown). This result indicates the presence of three distinct populations without exchange phenomena in the time scale of the analysis. A 18.5% water content corresponds to 227 g water per kg of dry clay. This corresponds to the value of 220 g water per kg of dry MX80 bentonite measured by Devineau et al (2006) for a relative humidity of 98%. The calculated amount of surface water for one kg of dry clay is 254 g. This value is in good agreement with the measured value (227 gw) and one can consider the clay material fully hydrated. The NMR results give a distribution of 6 (1 ms) / 85 (0.5 ms) / 9 (0.2 ms) between the different T_2 populations. A three-layer hydrate on the external surface would correspond to about 27 g of water per kg of dry clay i.e. 10% of the available water. This value would correspond to the T_2 population proportion having the highest value and thus the highest mobility (6%). Iwasaki and Takashi (1988) showed that Na/Ca-smectites tend to segregate into a mixture of Na-smectite and Ca-smectite. The two other T_2 water populations are therefore expected to belong to interlayer cations with different water mobilities (different numbers of bound water molecules) and relaxation properties e.g. Na interlayers (18%) vs. Ca or Mg (72%) interlayers. The results are therefore consistent with quantitative values in the range of those experimentally measured.

Synthetic Na-montmorillonite exhibited only two T_2 values, indicating the presence of only two populations of water. Based on the results obtained with MX-80 bentonite, we attributed these populations to external and internal surface water layers. A water content of 28.3%

corresponds to a mass of water of 395 g per kg of dry clay. This is higher than the content of adsorbed water observed by Michot et al. (2002) on Na-montmorillonite (287) for a relative humidity of 100%, but uncertainties close to RH = 100% are large due to potential liquid water condensation. Assuming that 31 and 99 g water per kg dry clay are necessary to create one molecular layer of water on the external and interlayer surfaces respectively, this amount of water experimentally determined corresponds to 3 layers of water on the entire surface. The material appears therefore fully hydrated since 3 layers were expected (part 2.3.3). Using the characteristics of the clay material (Table 1), one expects a distribution of 76 / 24 for interlayer and external water, respectively. The relative proportions of the two T_2 populations (83 / 17) correspond well with those expected. Furthermore, as for MX-80, the external population is characterized by a higher mobility than that of the internal population.

Finally, it is worth noting that the relaxation time values obtained are higher for synthetic montmorillonite than for MX-80 bentonite. With the exception of the interlayer composition, whose effect has been discussed above, the main difference between the two clay materials is the absence of iron in the synthetic montmorillonite structural formula. These relaxation time differences are notably due to the effect of variations in the magnetic susceptibility within samples or to the presence of paramagnetic or ferromagnetic species (Levin et al., 2007, Plassais et al., 2003, Chen et al., 2005); the surface of mineral grains is a strong relaxation sink (Nakashima, 2004).

3.1.3. NMR results on consolidated, water-saturated porous clay samples

The systems studied are presented in Table 4. The total porosities obtained from the percentage of water measured from the FID signal correspond well with the values calculated using the volumetric masses of the clay materials.

NMR results on consolidated, water-saturated porous clay samples exhibit the same number of T_2 values (water populations) as on the hydrated samples. For illite, T_2 increases with the moisture content of the sample (compare the results in Tables 3 and 4). This is coherent with the occurrence of a fast exchange phenomenon between external water molecules of the first and following layers, as discussed before for hydrated illite. Thus, as the water content increases, the proportion of the most mobile fraction increases leading to an increase in the mean relaxation time. As a consequence, it is also impossible to distinguish between external surface and bulk (in macroporosity) water from the analysis of the relaxation time curves at room temperature in compacted clay.

However, two important parameters are expected to differentiate surface and bulk water populations: the salt concentration and the proximity of the surface. Both parameters are known to affect the freezing temperature (Valckenborg et al., 2001). In conditions where bulk water can be selectively frozen, it is possible to make a distinction from the relaxation time values considering the great difference in mobility of the protons of ice ($T_2^* = 5\text{-}15$ μs) and of non-freezing water in a semi-liquid state. A typical experiment is presented in Figure 4, where the temperature was varied from +20°C to –25°C.

The most interesting results were obtained for T= -25°C and are presented in Table 4. As expected, two populations of water could be determined, one characterized by a very short relaxation time, $T_2 \approx 15$ μs (frozen water), the other by a longer relaxation time (semi-liquid water). Given that the FID water content value is coherent with the water content expected from the volumetric mass of the material (Table 4), it is then possible to quantify the amount of water affected by the vicinity of the surface by NMR.

For an illite sample saturated with Na, the amount of FID non-freezable water is 129 g water per kg of dry clay. This corresponds to 3.3 layers of water on the external surface of the particles. For a MX80 sample equilibrated with synthetic ground water, the amount of non-

freezable FID water amounts to 204 g water per kg of dry clay and corresponds to 2.1 water layers on the surface of the material. A value of 2.8 can be calculated according to eq.(14). For the Ca-saturated synthetic montmorillonite in 0.1 M $CaCl_2$ solution, 24% of the total FID water does not freeze at -25°C. The non-freezable water then amounts to 260 g per kg of dry clay. This amount of water corresponds to 2 layers of water covering all of the surfaces (basal, edges and interlayers) whereas a value of 3 is calculated.

In conclusion, considering the starting assumptions described in part 2.3.3., an estimation of the fraction of surface water can be obtained at -25°C with a deviation of ± 10-30% with respect to the calculated values.

3.2. HTO and iodide accessible porosities

3.2.1 Comparison of HTO accessible porosity and NMR results

The evolution of the tritium radioactivity in the water-saturated porous media is presented in Figure 5 as a function of time. It can be explained by a diffusion controlled process. At equilibrium, the water content was determined and is given in Table 4.

These latter values are in good agreement with those obtained from the FID (H_2O) signal. The whole pore volume is therefore probed by HTO showing that the pores are connected.

The corresponding porosities calculated according to eq. (12) are in good agreement with the theoretical porosity (eq. (10)) using the volumetric mass of the clay. The simplifying assumption to consider a volumetric mass of water of 1000 kg/m^3 is therefore confirmed in the limit of the measurement precision. It may be noted that adsorbed water locally has a density above one (see for example molecular dynamics results from Wang et al. 2006 or Tournassat et al., 2009b) but this density must be similar to 1000 kg/dm^3 when normalized to three layers of external water, taking into account the density oscillations with domains also at density below 1000 kg/m^3.

This result further validates our simplifying assumption used to treat the isotopic dilution data, i.e. to consider the concentration of the components, and not the chemical potential, equal in the different parts of the system at equilibrium.

3.2.1 Comparison of iodide accessible porosity and NMR results

Results of the isotopic dilution experiments performed with iodide are presented in Figure 5. About 1 day was necessary to reach equilibrium. As for HTO, the data is well explained by a diffusion process. Porosities can be obtained providing that iodide sorption can be neglected (see eq. 3). The sorption of iodide on synthetic montmorillonite and MX-80 bentonite can be neglected (Kaplan et al., 2000). For illite, in conditions relevant to nuclear waste repositories in clay formations (pH~7, ionic strength ~ 0.1 M), contradictory results are found in the literature: it is considered either significant with Kd values around 20 L/kg (Kaplan et al., 2000) or weak with Kd values expected below 1 L/kg (Tournassat et al., 2007). To assess the importance of this sorption parameter, porosities were estimated for the two model phases as a function of parameters affecting sorption, i.e. iodide concentration (pH=7, Figure 6A) and pH value (trace concentration, Figure 6B), and they were compared with the accessible porosities estimated for Cl^-, which is considered as a conservative tracer (Bradbury and Baeyens, 2003b). For both illite and synthetic montmorillonite, no significant effect is observed when iodide concentration varies. Furthermore, porosities estimated for iodide and chloride are similar. For illite, a slight but significant effect is observed for trace concentrations of iodide when the pH value is varied: the porosity increases as the pH decreases. In conclusion, for pH<5 and for trace concentrations of iodide (10^{-7}M), a sorption is observed for illite. The calculated Kd values vary from 0.02 to 0.09 L/kg. On the one hand, these values appear much lower than those proposed by Kaplan et al. (2000) with values varying between 46 to 22 L/Kg as the pH value increased from 3.6 to 9.4. On the other hand, these values appear coherent

with the work of Tournassat et al. (2007). For $[I^-]>10^{-6}$ M and for the pH range studied (4-8), the sorption can be neglected for both illite and synthetic montmorillonite. In these conditions, the accessible porosities for iodide can be determined. Based on these results, the conditions chosen for MX-80 bentonite and purified illite were pH=7, [NaI]=0.01 M.

Unlike HTO, the isotopic dilution data for iodide cannot be compared directly with NMR results. While the total exclusion from interlayer water is a reasonable assumption that can be linked directly to the NMR results, the exclusion volume at the external surfaces is mainly linked to electrostatic parameters without any straightforward link with the water probed by NMR, although it is expected to be located in the double layer where the ionic strength is higher than in the bulk water (see part 3.1.3.).

To allow a comparison with experimental porosities, we applied the modified Gouy-Chapman (MGC) theory to calculate the anion exclusion distance according to the method given in Sposito (1992). Using this approach, equivalent anion exclusion distances are 18 Å at I = 0.1 and 10 Å at I = 0.3 for a smectite surface with surface charge of -0.72 protonic charge per nm^2. For an illite surface, with a surface charge of -0.18 protonic charge per nm^2, the calculated anion exclusion distance is about 20 Å at I = 0.1 and 12 Å at I = 0.3. As a consequence, at I=0.3, the anion exclusion distance is expected to be similar to the volume occupied by 3-4 layers of water. It should be noted that the MGC approach has been used here for a divalent salt background as well as for a NaCl salt background, although this approach has been proven to be accurate only for NaCl in dilute systems (e.g. Sposito, 1992).

For Ca-SM, the volume accessible to iodide corresponds to 71±7% of the total water volume. This volume is in good agreement with the volume of frozen water (at -25°C) determined by NMR (Table 4). The remaining volume of non-frozen water is mainly constituted by interlayer water (76%, see part 3.1.2). On the one hand, this result provides strong indirect evidence of the exclusion of iodide from the interlayer in our experimental conditions. On the

other hand, the measurement precision prevents us from stating clearly if the MGC approach accurately predicts the anion exclusion at the external surfaces: the calculated volume of exclusion on external surface is 9% of total volume, compared with the measured total exclusion volume of 29±7%. A similar conclusion was obtained with MX-80.

For illite, while HTO tracer dilution results are in very good agreement with NMR results (Table 4), the volume of water accessible to iodide is slightly higher (87±6% of total volume) than the frozen water volume at -25°C (75±4%). The contrary was rather expected: the non-frozen water volume is equivalent to approximately three layers of water on the illite surface that is itself less than the exclusion volume predicted from the MGC model (20 Å ~ 6-7 layers of water). This result is surprising, because the experimental conditions are within the limit of applicability of the MGC theory (NaCl salt background and ionic strength below 0.1). The departure from the model can be interpreted either as (i) a geometric effect due to the consolidated state of the material (diffuse layer overlaps) or (ii) an inaccuracy of the model in our experimental conditions. In the experimental conditions (dry density = 1274 kg/m^3, [NaCl] = 0.1 mol/L, specific illite surface area = 130 m^2/g), the MGC model predicts a total exclusion volume of 0.33 m^3/m^3 that is significantly less than the total porosity of the system (0.53, Table 4). As a consequence, the first hypothesis cannot easily explain by itself the observed discrepancy, which must also be seen as a departure from our MGC model parameters. In particular, illite surface could exhibit exchanged cations in inner-sphere complexes, lowering the expected surface potential and the anion exclusion volume. MGC model calculations show that this hypothesis would imply that less than 4% of the charge would be compensated in the diffuse layer, 96% of the charge being already compensated by inner-sphere complexes.

4. SUMMARY AND CONCLUSIONS

Using the NMR-FID signal, it was possible to probe both –OH (structural) and H_2O entities. The quantification of the number of OH groups is not precise owing to the very short relaxation time characterizing these protons. The experimental value underestimates the theoretical value, with a deviation of about 40%. The analysis of the CPMG relaxation curve sequence enables the determination of the forms of surface water molecules in "compartments" where no exchange phenomenon exists with each other in the timescale of NMR measurements. Only one water population (external surface water) could be determined for illite. For synthetic montmorillonite and MX-80 bentonite, it was possible to differentiate surface water belonging to external and internal surfaces and to differentiate distinct interlayers with different interlayer cations. The NMR technique appears suitable for distinguishing between surface and bulk water (with an uncertainty of ~ 10-30%) providing that the measurement is performed at –25°C. In these conditions, surface water remains semi-liquid whereas bulk water freezes. In our experimental conditions (I=0.1-0.3), about three layers of water at the external surfaces of clay minerals does not freeze at -25°C. This number of water layers corresponds to the usually reported number of significantly structured layers at the clay mineral water interface.

When the surface water volume is mainly constituted of interlayer water (case of montmorillonite and bentonite), anions such as iodide are excluded from a volume equal to that of surface water, giving sense to the dual-porosity models currently developed for the diffusion of anions in compacted clay materials (e.g. Bourg et al., 2006). When the interlayer water was not present (case of illite), the results show that iodide could access a small fraction of the surface water volume localized at the external surface of the clay particles. In the framework of the MGC theory and associated anion exclusion distance calculation, this result

could be explained by the adsorption of most of the counter-balancing sodium cations in inner-sphere complexes at the illite surface.

ACKNOWLEDGMENTS

This work was financed by the European Commission, within the framework of the FUNMIG integrated project and the ACTINET network of excellence (project n° 05-21), and the French National Agency for Radioactive Waste Management (ANDRA). We thank J. Brendle (Laboratoire de Matériaux à Porosité Contrôlée, Mulhouse, France) for providing the synthetic montmorillonite and F. Villieras (Laboratoire Environnement et Minéralurgie, Nancy, France) for determining the specific surfaces of illite. Pr. Sparks, Associate Editor, Ian Bourg and two anonymous referees are gratefully acknowledged for their useful comments and suggestions on the manuscript.

REFERENCES

Abragam A. (1961) The principles of Nuclear Magnetism, Oxford University Press Ed.

Alba M.D., Becerro A.I., Castro M.A., Perdigon A.C. and Trillo J.M. (2003). Inherent acidity of aqua metal ions in solids: an assay in layered aluminosilicates. *J. Phys. Chem. B* **107**, 3996.

Al-Mahrooqi S. H., Grattoni C. A., Muggeridge A. H., Zimmerman R. W., Jing X. D. (2006) Pore-scale modelling of NMR relaxation for the characterization of wettability. *J. Petrol. Sci. Eng.* **52**, 172.

Andra (2005) Dossier 2005 argile; Référentiel de comportement des radionucléides et des toxiques chimiques d'un stockage dans le Callovo-Oxfordien jusqu'à l'homme. Tome 1. Andra report C.RP.ASTR.04.0032.A.

Appelo, C.A.J., Wersin, P. (2007) Multicomponent diffusion modeling in clay systems with application to the diffusion of tritium, iodide, and sodium in Opalinus clay. *Environ. Sci. Technol.* **41**, 5002.

Appelo, C.A.J., Vinsot, A., Mettler, S. and Wechner, S. (2008) Obtaining the porewater composition of a clay rock by modeling the in- and out-diffusion of anions and cations from an in-situ experiment. *J. Contam. Hydrol.* **101**, 67.

Barrie P.J. (2000) Characterization of porous media using NMR methods. Annual Reports on NMR Spectroscopy, Vol. 41, Webb G.A. Ed., Academic Press.

Bardot F., Villiéras F., Michot L. J., François M., Gérard G. and Cases J. M. (1998) High resolution gas adsorption study on illite permuted with various cation: Assessment of surface energetic properties. *J. Disp. Sci. Technol.* **19**, 739.

Bertram H. C., Andersen H. J., Karlsson A. H. (2001) Comparative study of low-field NMR relaxation measurements and two traditional methods in the determination of water holding capacity of pork. *Meat Sci.* **57**, 125.

Bourg, I.C. (2004) Tracer diffusion of water and inorganic ions in compacted saturated sodium bentonite, pH-D report, University of California, Berkeley.

Bourg, I.C., Sposito, G., Bourg, A.C.M. (2006) Tracer diffusion in compacted, water-saturated bentonite. *Clay. Clay. Miner.* **54**, 363.

Bourg I.C., Sposito G., Bourg A.C.M. (2007) Modeling the acid-base surface chemistry of montmorillonite. *J. Colloid Interface Sci*. **312**, 297.

Bradbury M.H., Baeyens B. (1997) A mechanistic description of Ni and Zn sorption on Na-montmorillonite. Part II: Modelling. *J. Contam. Hydrol.* **27**, 223.

Bradbury M.H., Baeyens B. (2003a) Near field sorption data bases for compacted MX-80 bentonite for performance assessment of a high-level radioactive waste repository in opalinus clay host rock. PSI Report N. 03-07, Villigen.

Bradbury M.H., Baeyens B. (2003b) Porewater chemistry in compacted re-saturated MX-80 bentonite. *J. Contam. Hydrol.* **61***,* 329.

Bradbury M.H., Baeyens B. (2005) Experimental and modelling investigations on Na-illite: Acid-base behaviour and the sorption of strontium, nickel, europium and uranyl. PSI report Nr. 05-02, Villigen.

Cases J.M., Berend I., Francois M., Uriot J.P., Michot L.J., Thomas F. (1997) Mechanism of adsorption and desorption of water vapor by homoionic montmorillonite; 3, the Mg^{2+}, Ca^{2+} and Ba^{2+} exchanged forms. *Clays and Clay Minerals* **45**, 8.

Chavez-Paez, M., dePablo, L., dePablo, J.J. (2001) Monte Carlo simulations of Ca-montmorillonite hydrates. *J. Chem. Phys.* **114**, 10948.

Chen Q., Marble A.E., Colpitts B.G., Balcom B.J. (2005) The internal magnetic field distribution, and single exponential magnetic resonance free induction decay, in rocks. *J. Mag. Reson.* **175**, 300.

Dennis J. E., Gay D. M., Welsh R. E. (1981) An Adaptive Nonlinear Least-. Squares Algorithm. *ACM Trans. Math. Software* **7**, 3.

Devineau K., Bihannic I., Michot L., Villiéras F., Masrouri F., Cuisinier O., Fragneto G., Michau N. (2006) In situ neutron diffraction analysis of the influence of geometric confinement on crystalline swelling of montmorillonite. *Applied Clay Science* **31,** 76.

Ernst R. R., Bodenhausen G., Wokaun A (1987) In: Principles of NMR in one and two dimensions, § 4.2.2 and 4.2.3., Clarendon press, Oxford.

Ferrage, E., Lanson, B., Sakharov, B.A., Drits, V.A. (2005) Investigation of smectite hydration properties by modeling experimental X-ray diffraction patterns: Part I. Montmorillonite hydration properties. *Am. Mineral.* **90**, 1358.

Ferrage, E., Kirk, C.A., Cressey, G., Cuadros, J. (2007) Dehydration of Ca-montmorillonite at the crystal scale. Part I: Structure evolution. *Am. Mineral.* **92**, 994.

Gabis V. (1958) Etude préliminaire des argiles oligocènes du Puy-en-Velay (Haute-Loire). *Bull. Soc. Franç. Minér. Crist.* **LXXX**I, 183.

Gaucher E.C., Blanc P., Bardot F., Braiban, G., Buschaert S., Crouzet C., Gautier A., Girard J.-P., Jacquot E., Lassin A., Negrel G., Tournassat C., Vinsot A., Altmann S. (2006) Modelling the porewater chemistry of the Callovian-Oxfordian formation at a regional scale. *C.R. Geosci.* **338**, 917.

Ghosh A., Smits M., Bredenbeck J., Bonn M. (2007) Membrane-bound water is energetically decoupled from nearby bulk water: an ultrafast surface specific investigation. *J. Am. Chem. Soc.* **129**, 9608.

Greathouse, J.A., Cygan, R.T. (2006) Water structure and aqueous uranyl(VI) adsorption equilibria onto external surfaces of beidellite, montmorillonite, and pyrophyllite: Results from molecular simulations. *Environ. Sci. Technol.* **40**, 3865.

Guichet X., Fleury M., Kohler E. (2008) Effect of clay aggregation on water diffusivity using low field NMR, *J. Colloid Interface Sci.* **327**, 84.

Hansen E. W., Gran H. C., Johannessen E. (2005) Diffusion of water in cement paste probed by isotopic exchange experiments and PFG NMR. *Micropor. Mesopor. Mat.* **78**, 43.

Hills B. P. (2006) Applications of low-field NMR to food science, *Annual Reports on NMR Spectroscopy* **58**, 177.

Hirama Y., Takahashi T., Hino M., Sato T. (1996) Studies of water adsorbed in porous Vycor glass, *J. Colloid Interface Sci*. **184**, 349.

Iwasaki T., Takashi T. (1988) Distribution of Ca and Na Ions in Dioctahedral Smectites and Interstratified Dioctahedral Mica/Smectites. *Clays Clay Miner. 36,* 73.

Kaplan D. I., Jeff Serne R., Parker K. E., Kutnyakov I. V. (2000) Iodide sorption to subsurface and illitic minerals, *Environ. Sci. Technol.* **34**, 399.

Korb J.-P., Godefroy S., Fleury M. (2003) Surface nuclear magnetic relaxation and dynamics of water and oil in granular packings and rocks. *Mag. Reson. Imaging* **21**, 193.

Kowalczyk P., Terzyk A.P., Gauden P.A. (2002) The application of a Contin package for the evaluation of micropore size distribution functions. *Langmuir* **18**, 5406.

Kozaki T., Fujishima A., Sato S., Ohashi H. (1998) Self-diffusion of sodium ions in compacted sodium montmorillonite. *Nucl. Techn.* **121**, 63.

Le Botlan D. J., Ouguerram L. (1997) Spin-spin relaxation time determination of intermediate states in heterogeneous products from free induction decay NMR signals. *Anal. Chim. Acta* **349**, 339.

Le Botlan D., Rugraff Y., Martin C., Colonna P. (1998) Quantitative determination of bound water in wheat starch by time domain NMR spectroscopy. *Carbohydr. Res.* **308**, 29.

Levin E.M., Bud'ko S.L., Mao J.D., Huang Y., Schmidt-Rohr K. (2007) Effect of magnetic particles on NMR spectra of Murchison meteorite organic matter and a polymer-based model system. *Solid State Nucl. Mag. Reson*. **31**, 63.

Manalo F. P., Kantzas A., Langford C. H. (2003) Soil wettability as determined from using low-field nuclear magnetic resonance. *Environ. Sci. Technol.* **37**, 2701.

Marry, V., Rotenberg, B., Turq, P. (2008) Structure and dynamics of water at a clay surface from molecular dynamics simulation. *Phys. Chem. Chem. Phys.* **10**, 4802.

Marty, N.C.M. (2009) Influence of dissolution/precipitation kinetics on the porosity clogging effect during cement/clay interaction. Report BRGM/RP-56236-FR.

Meiboom S., Gill D. (1958) Modified spin-echo method for measuring nuclear relaxation times. *Rev. Sci. Instr.* **29**, 688.

Michot L.J., Villiéras F., François M., Bihannic I., Pelletier M.,Cases J.M. (2002) Water organisation at the solid-aqueous solution interface. *C.R. Geoscience* **334**, 611.

Mitchell J., Stark S.C., Strange J.H. (2005) Probing surface interactions by combining NMR cryoporometry and NMR relaxometry. *J. Phys. D: Appl. Phys.* **38**, 1950.

Mitchell J., Webber J.B.W., Strange J.H. (2008) Nuclear magnetic resonance cryoporometry. *Physics Reports* **461**, 1.

Montavon G., Alhajji E., Grambow B. (2006) Study of the Interaction of $Ni^{2+}$and Cs^{+} on MX-80 Bentonite; Effect of Compaction Using the "Capillary Method". *Environ. Sci. Technol.* **40**, 4672.

Nakashima Y. (2004) Nuclear magnetic resonance properties of water-rich gels of Kunigel-V1 bentonite. *J. Nucl. Sci. Technol.* **41**, 981.

Parkhurst D.L., Appelo C.A.J. (1999) User's guide to phreeqc—a computer program for speciation, batch-reaction, one-dimensional transport, and inverse geochemical calculations, USGS Report No. 99-4259.

Plassais A., Pomiès M.-P, Lequeux N., Boch P., Korb J.-P., Petit D., Barberon F. (2003) Micropore size analysis by NMR in hydrated cement. *Mag. Reson. Imaging* **21**, 369.

Porion P., Faugère A.M., Levitz P., Van Damme H., Raoof A., Guilbaud J.P., Chevoir F. (1998) A NMR investigation of adsorption/desorption hysteresis in porous silica gels. *Mag. Reson. Imaging* **16**, 679.

Provencher S. (1982) A constrained regularization method for inverting data represented by linear algebraic or integral equations. *Comput. Phys. Commun.* **27**, 213.

Reinholdt M., Miehé-Brendlé J., Delmotte L., Le Dred R., Tuilier M.-H. (2005). Synthesis and characterization of montmorillonite-type phyllosilicates in a fluoride medium. *Clay Minerals* **40**, 177.

Sato, T., Watanabe, T., Otsuka, R. (1992) Effects of layer charge, charge location, and energy change on expansion properties of dioctahedral smectites. *Clay. Clay. Miner.* **40**, 103.

Sauzéat E., Guillaume D., Villiéras F., Dubessy J., François M., Pfeiffert C., Pelletier M., Ruck R., Barrès O., Yvon J., Cathelineau M. (2001) Caractérisation minéralogique, cristallochimique et texturale de l'argile MX-80, ANDRA report C RP 0LEM 01-001.

Snaar J. E. M., Hills B. P. (1995) Water proton relaxation studies of air-water distributions in beds of randomly packed monodisperse glass microspheres. *Mol. Phys.* **86**, 1137.

Sposito G., Prost P. (1982) Structure of water adsorbed on smectite. *Chem. Rev.* **82**, 553.

Sposito, G. (1992) The diffuse-ion swarm near smectite particles suspended in 1:1 electrolyte solutions: modified Gouy-Chapman theory and quasicrystal formation. In: N. Güven and R.M. Pollastro (Editors), Clay-water interface and its rheological implications. Clay minerals society, pp. 127-156.

Tambach, T.J., Hensen, E.J.M., Smit, B. (2004) Molecular simulations of swelling clay minerals. *J. Phys. Chem. B* **108**, 7586.

Todoruk T. R., Langford C. H., Kantzas A. (2003) Pore-scale redistribution of water during wetting of air-dried soils as studied by low-field NMR relaxometry. *Environ. Sci. Technol*. **37**, 2707.

Tournassat C., Ferrage E., Poinsignon C., Charlet L. (2004). The titration of clay minerals I. Discontinuous backtitration technique combined with CEC measurements. *J. Colloid Interface Sci.* **273**, 224.

Tournassat, C., Gaucher E.C., Fattahi M., Grambow B. (2007) On the mobility and potential retention of iodine in the Callovian–Oxfordian formation. *Phys. Chem. Earth, Parts A/B/C* **32**, 539.

Tournassat, C., Gailhanou, H., Crouzet, C., Braibant, G., Gautier, A., Gaucher, E.C. (2009a) Cation exchange selectivity coefficient values on smectite and mixed-layer illite/smectite minerals. *Soil Sci. Soc. Am. J.* **73**, 928.

Tournassat, C., Chapron, Y., Leroy, P., Bizi, M. and Boulahya, F. (2009b), Comparison of molecular dynamics simulations with Triple Layer and modified Gouy-Chapman models in a 0.1 M NaCl - montmorillonite system. *J. Colloid Interf*ace Sci., **doi:10.1016/j.jcis.2009.06.051**.

Valckenborg R., Pel L., Kopinga K. (2001) Cryoporometry and relaxometry of water in silica-gels. *Magn. Reson. Imaging* **19**, 489.

Van Loon, L.R., Glaus, M.A., Müller, W. (2007) Anion exclusion effects in compacted bentonites: Towards a better understanding of anion diffusion. *Appl. Geochem.* **22**, 2536.

Wang J., Kalinichev A.G., Kirkpatrick, R.J. (2006) Effects of substrate structure and composition on the structure, dynamics, and energetics of water at mineral surfaces: A molecular dynamics modeling study. *Geochim. Cosmochim. Acta* **70**, 562.

Yu, J.-W, Neretnieks I. (1997) Diffusion and sorption properties of radionuclides in compacted bentonite. SKB report TR 97-12, Stockholm.

Zhuravlev L.T. (2000) The surface chemistry of amorphous silica. Zhuravlev model. *Colloids Surfaces A* **173**, 1.

Zimmerman J.R., Brittin W.E. (1957) Nuclear magnetic resonance studies in multiple phase systems: lifetime of a water molecule in an adsorbing phase on silica gel. *J. Phys Chem.* **61**, 1328.

Table 1: Characteristics of the clays. Data for MX-80 bentonite are taken from (Tournassat et al. 2004).

Acronym of the sample	Mineralogy of the sample	External surface (m^2/g)		Interlayer (or internal) surface (m^2/g)
		edge	basal	
MX-80	Montmorillonite [a*]	8.5	26.6	723
Ca(Na)-SM	Montmorillonite [b]	11	93	657
Na-ILL	Illite [c]	26**	104**	_

a $(Si_{7.96}Al_{0.04})(Al_{3.10}Fe^{3+}_{0.18}Fe^{2+}_{0.16}Mg_{0.56})O_{20}(OH)_4Na_{0.15}Mg_{0.15}Ca_{0.15}$ (Sauzeat et al., 2001)

b $(Si_{3.8}Al_{0.2})(Al_{1.67}Mg_{0.33})O_{10}(OH_{1.9}F_{0.1)}Na_{1.06})$

c $(Si_{3.52}Al_{0.48})(Al_{1.17}Fe^{3+}_{0.49}Mg_{0.33})O_{10}(OH_2)(Ca_{0.04}Na_{0.12}K_{0.64})$ (Bradbury et Baeyens, 2005)

* Content of 0.79 % (Andra, 2005)

** Measure after the treatment at pH 3

Table 2: Dried samples; NMR FID results obtained in H_2O and D_2O. a.u. arbitrary units.

	FID signal		**Results in D_2O (as mole of H/ kg of dry clay)**	
	T_2* (μs)	**I (a.u.)**	**Exchangeable part**	**Non-exchangeable part**
Na-ILL	21	295	0.4	3.3
	50-150	60	0.75	_
Na-SM	16	340	0.6	3.6
	50-150	380	4.8	_

Table 3: NMR results obtained for samples hydrated at a relative humidity of 100%. The values in brackets correspond to the distribution in T_2 values in %.

	Water content (%)	**CPMG; T_2 (ms)**
Na-ILL	8.8	0.3
Na-SM	28.3	6.3 (83) 11.3 (17)
MX-80	18.5	0.2 (9) 0.5 (85) 1.0 (6)

Table 4: Water-saturated and consolidated porous clay samples; NMR and tracer experiment results.

System characterization			NMR				Tracer experiments		
System	Dry density (in kg / m^3)	Corresponding theoretical total porosity *	Total porosity (FID signal)		Frozen water at -25°C	CPMG (20°C)	Total porosity (HTO)		Iodide
			Wc (NMR)	Corresponding porosity	(proportion in $\%H_2O$)		Wc (HTO)	Corresponding porosity	(HTO porewater volume probed in %)
Ca-SM / 0.1M $CaCl_2$	583	0.78	0.52 ±0.02	0.74 ± 0.03	76 ± 4	14 ms (56) 23.8ms (44)	0.52±0.05	0.74 ± 0.06	71± 7
MX-80 / SGW	1067	0.63	0.29 ± 0.01	0.54 ± 0.02	50 ± 3	n.m.	0.35±0.02	0.61 ± 0.03	49±8
Na-ILL / 0.1M NaCl	1274	0.53	0.34 ±0.0 1	0.58 ± 0.02	75 ± 4	1.52 ms	0.31±.0.02	0.55 ± 0.03	87±6

Footnotes: The dry density is given as kg of dry clay material per m^3 of volume occupied in the capillaries. The porosity corresponds to the volume of water divided by the total volume occupied by the porous clay system; * The volumetric mass of the synthetic montmorillonite, MX80 and illite are considered to be 2600, 2850 and 2700 kg/m^3 respectively, based on their structural formula. n.m. = not measured.

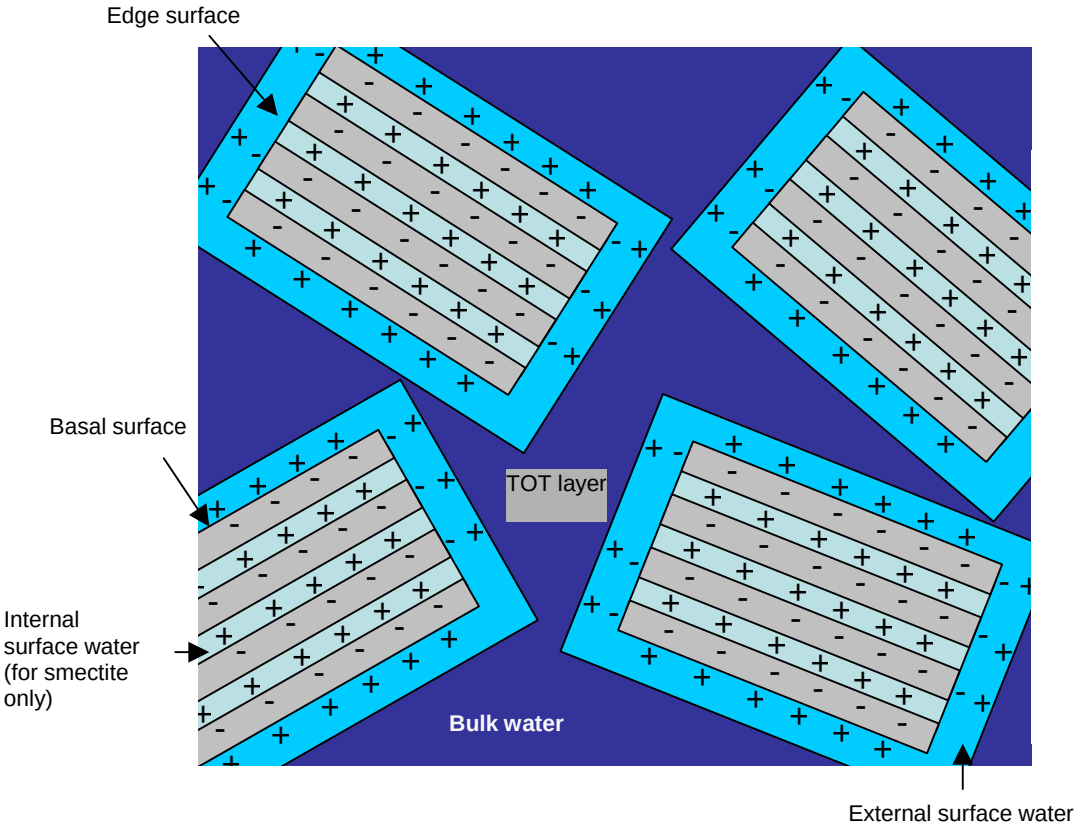

Figure 1: Water distribution on water-saturated compacted clay materials

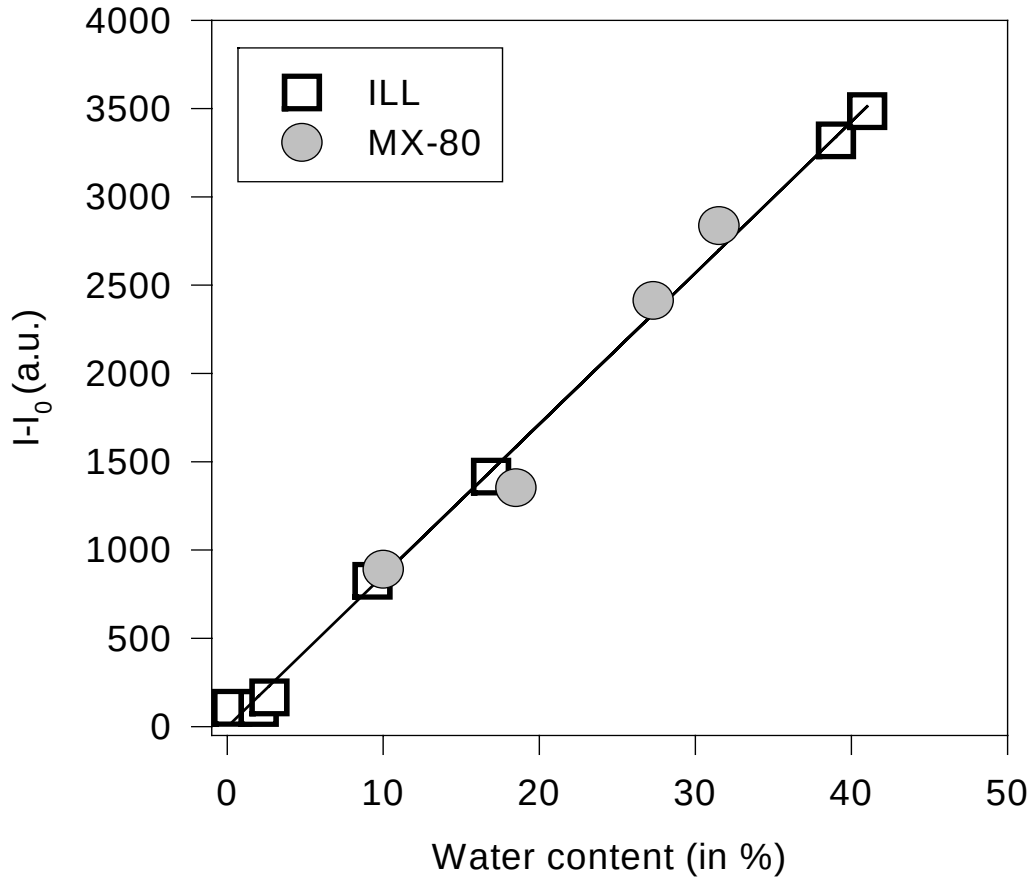

Figure 2: Quantitative relation between FID signal (see text) and water content.

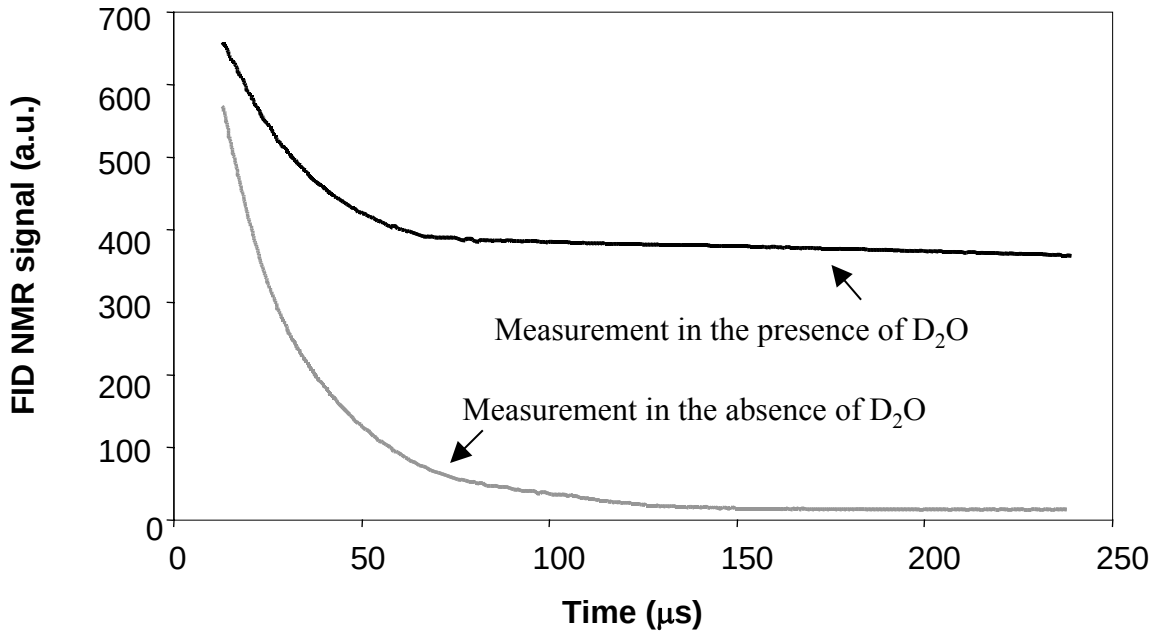

Figure 3: FID signal for dried Na-SM in the presence (upper curve) or absence (lower curve) of D_2O.

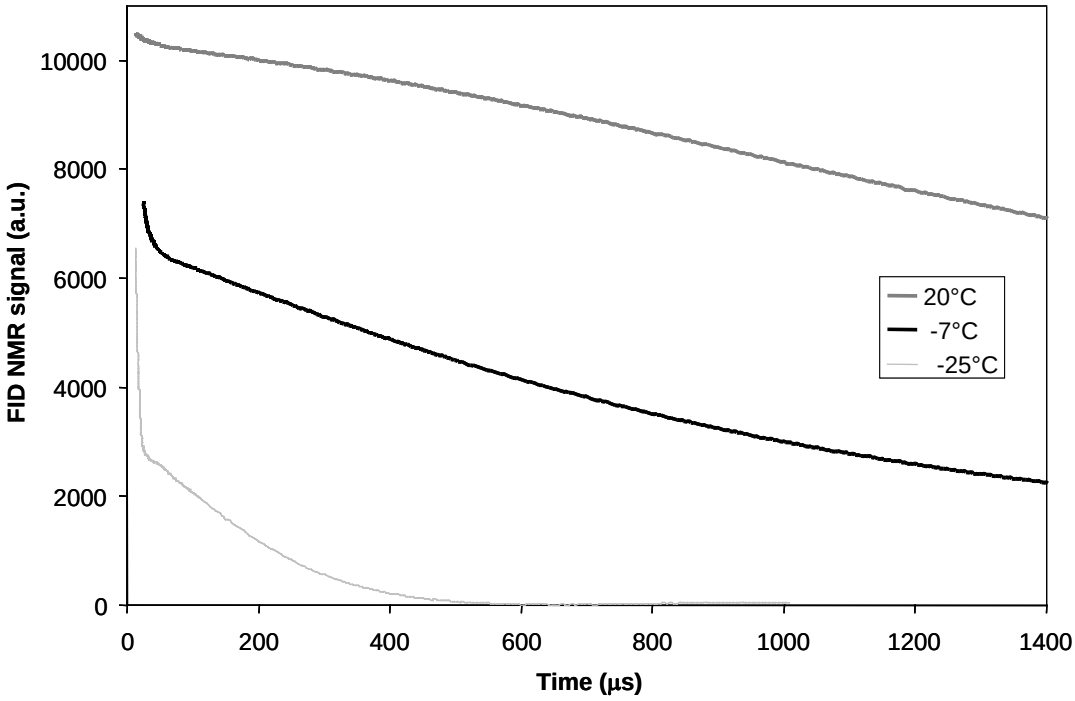

Figure 4: FID signal obtained for MX-80/SGW system as a function of temperature.

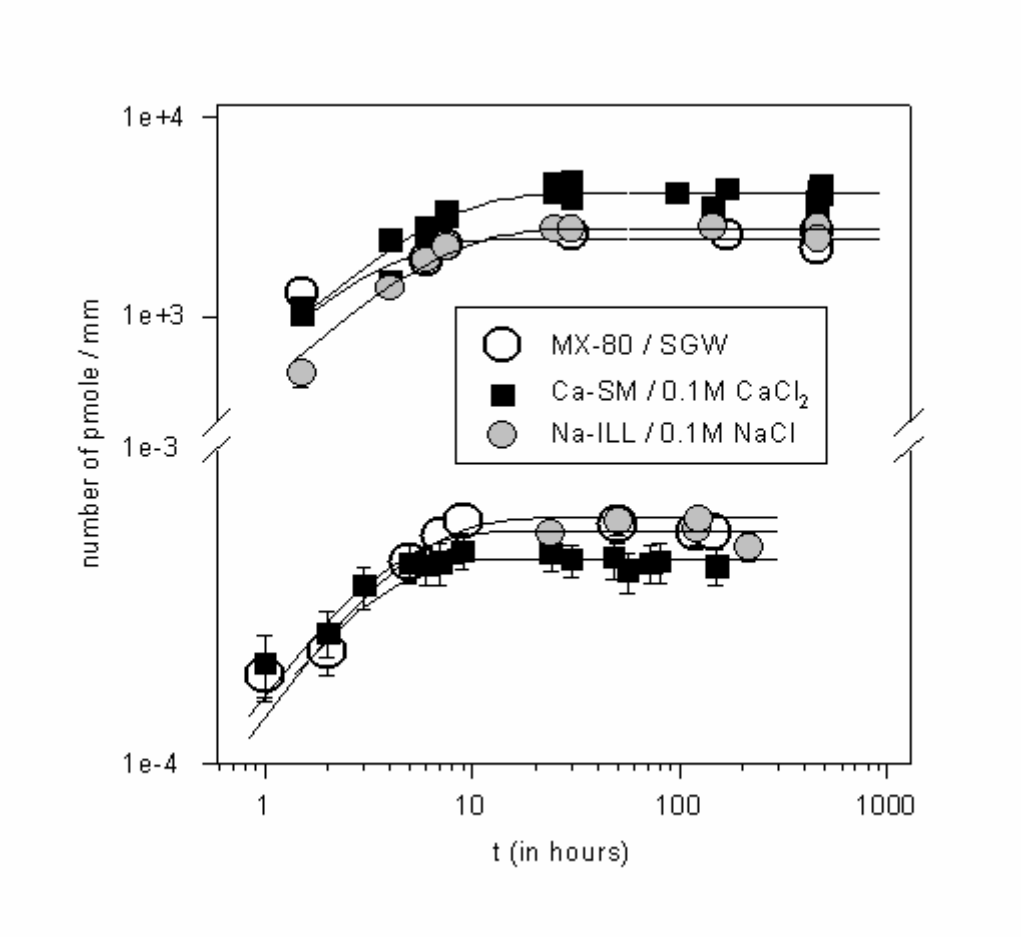

Figure 5: Isotopic dilution experiments performed with HTO (upper curves) and iodide (lower curves) for different systems of interest. Y axis represents the amount of HTO or I measured in the compacted medium at a given time (in picomoles) divided by the length of the compacted clay medium (in mm). The lines correspond to the calculation made considering a diffusion controlled process. For HTO, $D_e=4.10^{-10}$ m^2/s and porosities equal to 31, 53 and 25% for MX-80 Ca-SM and Na-ILL, respectively. For iodide, $D_e=3.10^{-10}$ m^2/s and porosities equal to 19, 40 and 19% for MX-80 Ca-SM and Na-ILL, respectively.

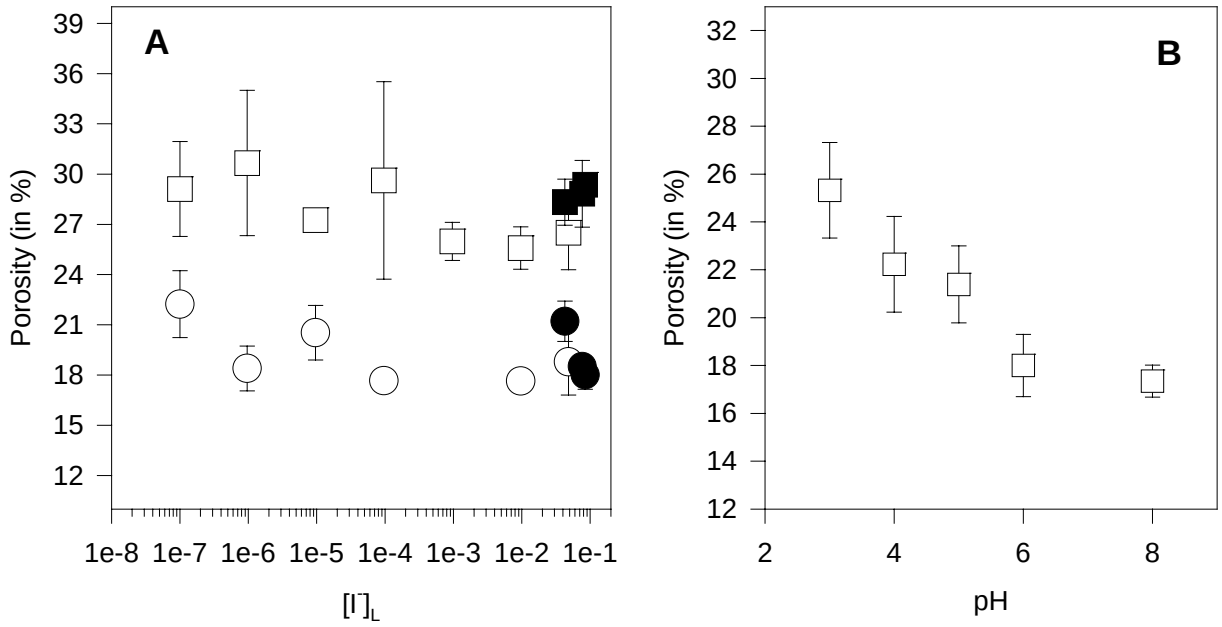

Figure 6: Porosity measurements for iodide (open symbols) and chloride (filled symbols) for Na-ILL (squares) and Na-SM (circles) systems as a function of iodide concentration **(A)** (pH=7) and pH **(B)** ([NaI]=10^{-7} M). The ionic strength was set at 0.1.

Figure SM-1 gives an example of residuals obtained for the fitting of the CPMG curve of MX-80 powder (14% water content); I_0=1220 a.u.